applied sciences

MDPI

Article

H_∞ Robust Load Frequency Control for Multi-Area Interconnected Power System with Hybrid Energy Storage System

Wenxu Yan, Lina Sheng, Dezhi Xu *, Weilin Yang and Qian Liu

School of Internet of Things Engineering, Jiangnan University, Wuxi 214000, China; ywx01@jiangnan.edu.cn (W.Y.); linasheng01@126.com (L.S.); ywl@jiangnan.edu.cn (W.Y.); pipingpaijing@163.com (Q.L.)

* Correspondence: xudezhi@jiangnan.edu.cn; Tel.: +86-0510-85912092

Received: 20 August 2018; Accepted: 19 September 2018; Published: 27 September 2018

Abstract: To enhance the quality of output power from regional interconnected power grid and strengthen the stability of overall system, a hybrid energy storage system (HESS) is applied to traditional multi-area interconnected power system to improve the performance of load frequency control. A novel topology structure of interconnected power system with the HESS is proposed. Considering the external disturbances of the system and the interconnected factors between each control area, the dynamic mathematical model of each area in the new topology is established in the form of state-space equation. Combining the state feedback robust control theory with linear matrix inequality (LMI) theory, the controller is designed to calculate how much power the HESS should provide to power grid in real time, according to the load change of system. Taking the four-area interconnected power system as study object, the simulation results obtained by MATLAB prove that the application of HESS can well improve the frequency stability of multi-area interconnected system and the H_∞ robust controller proposed in this paper is effective.

Keywords: load frequency control; multi-area interconnected power system; hybrid energy storage system; state feedback; H_∞ robust control; linear matrix inequality

1. Introduction

With the rapid development of new energy generation technologies such as photovoltaic power generation, wind power generation, et cetera, as well as user's growing requirement of power quality and power supply reliability, power system has changed from the traditional centralized large power grid to the multi-area interconnected power system [1]. The reliability, flexibility and economy of power grid can be greatly improved by the coordinated and optimal operation of regional interconnected power system. Moreover, it should not be ignored that the interconnection of regional power systems will increase the uncertainties and bring problems about the frequency stability in the power network [1–3].

A high-quality power system requires the power frequency rate and voltage of system to be kept within a certain range around the set value. This requirement can be reached by adjusting the active power and reactive power of the system. The load frequency control (LFC) is an important part of the automatic power generation control (AGC) in power system and the function of the LFC is to ensure the stability of power system load frequency [4,5]. In other words, the LFC is used to keep the balance between the generating power and user load. Specific assignments of the LFC are as follows: (1) Make sure that the deviation of load frequency can be maintained at zero. (2) The switching power between tie-lines can return to the set value quickly under any load variation disturbance [6]. The study of load

frequency stability control in power system began around the 1970s [7,8]. In pace with the development of LFC, the control mode has developed from only considering the load frequency stability into combining the load frequency with the tie-line exchanged power together [8–10]. The control object has also changed from a single generator to the whole power plant area, and from a single-area system to the multi-area interconnected power system [10]. Many scholars have been looking for methods to improve the control effect of the LFC, such as applying neural network theory, adaptive control, fuzzy control, predictive control and other optimal control theories. The chaos optimization algorithm is used to adjust the multi-area load frequency control PID controller in [11]. In [12], it is proposed to combine the adaptive modified bat algorithm with the fuzzy logic (FL) to set the parameters of the proportional controller on line to improve the control effect of the LFC. The particle swarm optimization (PSO) algorithm is applied to adjust parameters of the proposed PI controller in [13]. The uncertainty caused by the variation of governor and turbine parameters is considered in [14], and an adaptive model predictive control (AMPC) method is applied to the LFC controller for multi-area power systems which can change the object model in MPC structure online. However, the research on LFC optimization is not only reflected in the improvement of controller and algorithm. In [15], multiple controllable thyristors or synchronous series compensators are installed in multi-area power systems, improving the dynamic control effect of the LFC by the coordinated control of phase shifter.

The main contributions of this paper are as follows: (1) We propose a new diagram of four-area interconnected power system and establish the dynamic mathematical model of power system in each control area. (2) The HESS is introduced to provide the power flow in purpose of regulating the frequency and tie-line exchanged power of system. (3) We apply the generic mode control method in [16] to realize the charging and discharging of the HESS. (4) We design the H_∞ robust controller based on the LMI and state-feedback method to calculate how much power the HESS should provide to the power system. Through the analysis and comparison of simulation results from PID control, it is identified that the H_∞ controller can improve the stability of power frequency under external load disturbance and the HESS can convert the output power demand signal from the H_∞ controller into the corresponding power flow effectively.

This paper is organized as follows: in Section 2, a new topology diagram of four-area interconnected power system with the HESS is presented and concepts of the LFC and the HESS are introduced. Section 3 presents a detailed mathematical model of *i*th control area within the four-area interconnected power system in the form of state space equation. H_∞ state feedback controller is designed for power system with the HESS in the *i*th control area in Section 4, based on the mathematical model established in Section 3. Further simulation verification and results analysis of the method proposed in this paper are presented in Section 5. Finally, the conclusion is given in Section 6.

2. Multi-Area Interconnected Power System with the HESS

Interconnected power system is usually composed of several control areas. Each area is connected to another by a tie-line for power exchange under normal operating conditions to overcome the mismatch between the generation and the demand [17]. Under any load change disturbance, there are two control aims in the operation of interconnected power system model:

- One objective is to make sure that the deviation of load frequency is zero or fluctuate in a certain really small range near zero.
- Another objective is to ensure that the switching power of the tie line returns to the set value.

Taking the four-area interconnected power system as an example, a new topology diagram of interconnected power system with the HESS is presented in this paper which is shown in Figure 1 [6]. The regional power system consists of three parts: generation system, user load and the HESS. In Figure 1, “G” represents the generation system, “L” indicates the user load and the “H” denotes the hybrid energy storage system (HESS).

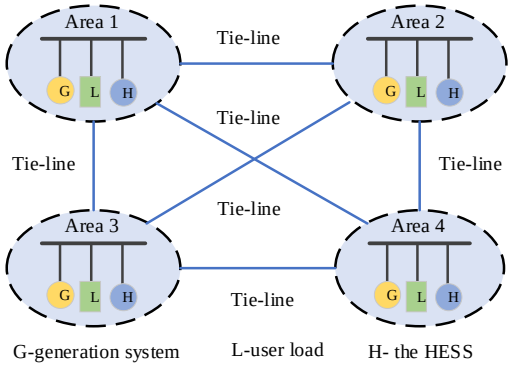

Figure 1. Topological structure diagram of four-area interconnected power system.

2.1. Load Frequency Control

Power system is a complex nonlinear dynamic system, because the power system is always affected by the load disturbance which results in the load frequency fluctuation [18]. In general, we use the method of near linearization to deal with the power system model. We usually adopt the linearization method near a certain working point to deal with the power system model [19,20]. A linear model is established to represent the dynamic model of system. The linearized model structure of system of *i*th control area in the interconnected power system is shown in Figure 2, which mainly includes the generator, the reheating turbine and the governor.

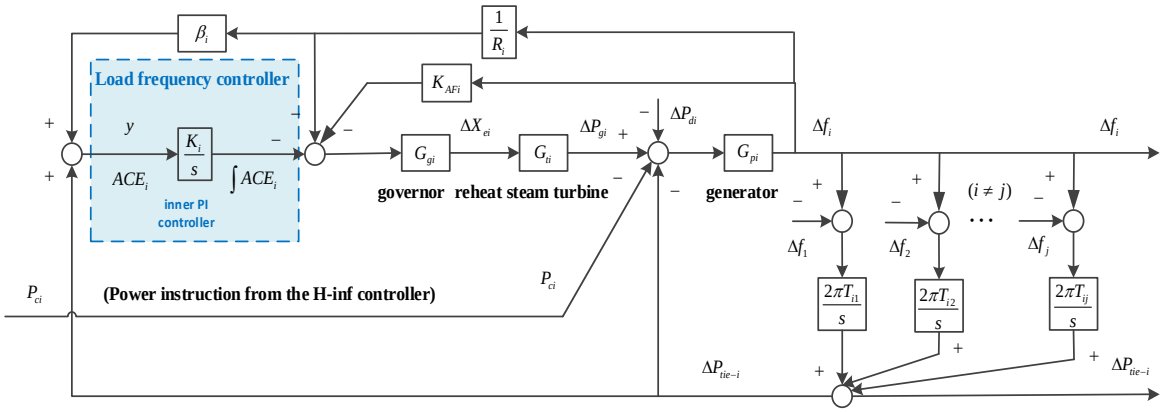

Figure 2. Linearization model structure of the system in *i*th control area.

The linearized model of the governor is as follows:

$$G_{gi} = \frac{1}{T_{gi}s + 1} \tag{1}$$

The linearized model of the reheat steam turbine is shown as:

$$G_{ti} = \frac{cT_{ri}s + 1}{(T_{ri}s + 1)(T_{ti}s + 1)} \tag{2}$$

The linearized model of the generator is as bellow:

$$G_{pi} = \frac{K_{pi}}{T_{pi}s + 1} \tag{3}$$

The physical implications of variables in the model of *i*th (i = 1,2,3,4) control area are as follows: T_{gi}, T_{ri}, T_{ti}, and T_{pi}, respectively, represent the time constant of governor, the reheating time constant,

the time constant of steam turbine and the time constant of power system. ΔX_{ei} indicates the incremental variation of governor valve position. ΔP_{ri} is the increment of output thermal power from reheat unit. ΔP_{tiei} denotes the deviation of power exchange between tie-lines. ΔP_{di} represents the load disturbance. Δf_i is the load frequency deviation of system. c is the reheating coefficient and K_{pi} is the gain of power system. T_{ij} represents the power synchronization coefficient of tie-line between the ith control area and the jth control area ($i \neq j$). K_{AFi} is the proportional negative feedback coefficient of the frequency deviation. φ_i denotes the frequency deviation constant that satisfies $\varphi_i = \beta_i / R_i$, where β_i is the set value of frequency deviation and R_i is the speed regulation gain.

To improve the power system with better dynamic performance, we should not only make sure that the frequency deviation (Δf_i) of the system tends to zero, but also ensure that the deviation of power exchange between tie lines (ΔP_{tiei}) is close to zero under any load disturbance. Considering the two targets above, the concept of area control error (ACE) is proposed in the LFC. The expression of ACE in the ith control area is formulated as (4):

$$ACE_i = \Delta P_{tiei} + \varphi_i \Delta f_i \tag{4}$$

In this paper, there is an internal PI controller in power system for frequency regulation which can be seen in Figure 2. The controlled variable u_{lfci} is as follows:

$$u_{lfci} = -\frac{K_i}{s} ACE_i \tag{5}$$

where K_i represents the control coefficient of PI regulation in ith control area.

Many works have been done to improve the control effect of the LFC and several novel control methods have been applied to the internal controller design in LFC. For example, the application of parameter self-adjusting algorithm to the PID controller [11,12] and the design of adaptive model predictive controller. In this paper, a hybrid energy storage system is introduced into traditional power system and an H_∞ robust state feedback controller is designed. The controller calculates the power supply in real time according to the variation of user load in system, and then the power control signal is transmitted to the HESS. The regulation of power in the system is realized by the effective charge and discharge of the HESS, which can ensure the stability of the load frequency.

2.2. Hybrid Energy Storage System

To guarantee the balance between the user power requirement and the active power generated by power grid, it is necessary to install the energy storage equipment with a certain capacity to adjust the power fluctuation of the power system. In the power system, the energy storage system is mainly used to calm down the fluctuating power of the system, reduce the sharp oscillation of system and cut down the peak and valley difference of the load power rate curve in purpose of enhancing the power quality [21–23]. We introduce the HESS into the inter-connected power system. The HESS aims to stabilize the load frequency of the power grid and eliminate a series of negative effects caused by the fluctuating power.

HESS is a kind of energy storage equipment composed of super capacitor (SC) and battery (B). The HESS has been proved theoretically that the structure can give full play to the characteristics of these two kinds of energy storage equipment by Dougal et al. in 2002 [24,25]. The SC has the characteristics of high power density, short charge and discharge time, high reliability and long cycle life. It is suitable for situations require high power, frequent electric charge and discharge instead of the battery with low energy density [22,25]. Nevertheless, the combination of SCs and batteries can not only meet the qualification of high power density and high energy density, but also can reduce the rated capacity of batteries and prolong its service life. Currently, the HESS has been widely regarded as an effective way to calm down the grid power fluctuation due to its technical and economic advantages [26,27].

The hybrid energy storage system (HESS) can be mainly divided into two categories: the passive HESS and the active HESS. In this paper, we choose an active parallel HESS comprised of super capacitors and Lithium-ion batteries. The basic structure of HESS is shown in Figure 3.

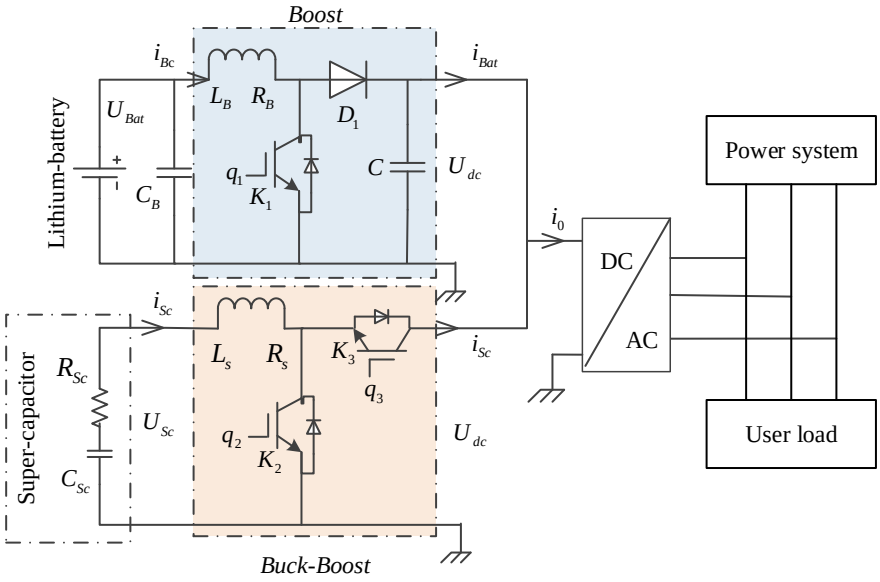

Figure 3. Basic structure of the hybrid energy storage system.

In Figure 3, the battery is connected with a boost converter and the supercapacitor is connected with a bi-directional DC-DC converter (buck-boost) [28]. Two converters share the same DC link which is connected to the power system through a DC-AC converter. As shown in Figure 3, the Lithium-ion battery part is composed of a inductance with high frequency L_B, an IGBT (Insulated-Gate Bipolar Transistor) K_1, a diode D_1 and an output filter capacitor C_B which plays a role in protecting the battery [29]. U_{Bat} is the voltage of the Lithium-ion battery. i_{Bc} is the inductor input current. i_{Bat} denotes the boost converter output current. U_{dc} represents the voltage of DC bus. The super capacitor part consists of a high frequency inductance L_{Sc} and two IGBTs K_2 and K_3; R_s and L_s represent the equivalent resistance and equivalent capacitance value of the super capacitor. U_{Sc} is the voltage of the SC. i_{Sc} is the inductor input current and it can be positive or negative. i_{Sc} is positive when the SC is in discharging mode. IGBT K_1, K_2 and K_3 respectively controlled by binary signal q_1, q_2 and q_2. The PWM signals for Lithium-ion battery and super capacitor are generated according to the energy-management strategy [16]. The power exchange between the HESS and power system can be seen in Figure 4.

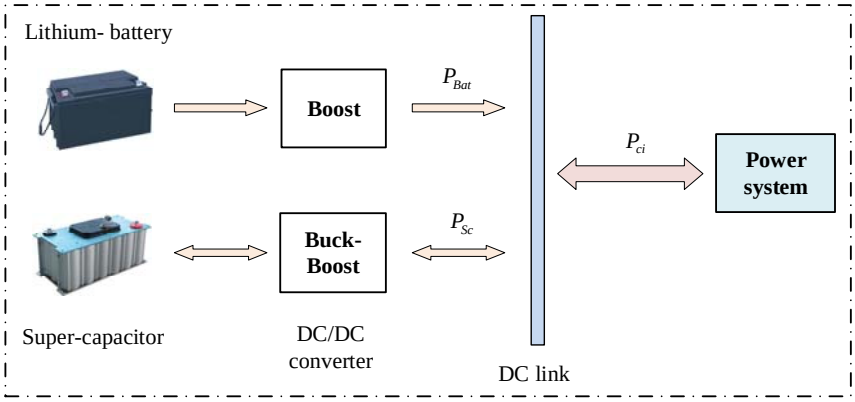

Figure 4. Power exchange between the HESS and power system.

P_{ci} represents the power requirement from power system corresponding to the output power instruction from the H_∞ state feedback controller designed in this paper. P_{Bat} and P_{Sc} are the power should be provided to power system by the battery and super-capacitor. Moreover, P_{Sc} is positive when the SC is in discharging mode and negative in charging mode. There are two working modes, namely, the voltage-reduction or charging mode and the boosting or discharge mode [30]. The power instruction P_{Sc} and P_{Bat} converted the corresponding current instruction i_{Sc} and i_{Bat} by calculation [16]. The HESS absorbs or emits corresponding power according to the difference value between the power generated by the power grid and the power required on the user side, thus the stabilization of frequency fluctuation power in power grid can be realized.

3. Mathematical Model of Power System with the HESS in the *i*th Control Area

State space description can effectively reveal and utilize the inner state information of the system. By this way, the complexity of mathematical representation will not be increased when the numbers of variables increase. In this paper, the mathematical model of *i*th control area within the four-area interconnected power system is established in the form of state space equation. To facilitate modeling, the linear expression of the reheat steam turbine (Equation (2)) is decomposed as shown in Figure 5. In Figure 5, ΔP_{gi} denotes the output power increment of power generation, ΔP_{ri} is the output thermal power increment of reheat unit and ΔX_{ei} indicates the incremental variation of governor valve position.

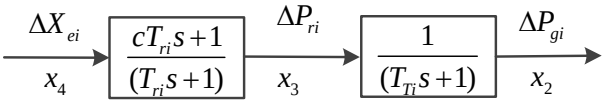

Figure 5. Transfer function of reheat steam turbine in the *i*th control area.

Thinking about the *i*th control area in a multi-area interconnected power system, define the output $y_i = ACE_i$, the input $u_i = P_{ci}$, inner state-space vector $x_i \in \mathbf{R}^{6\times1}$ and the disturbance vector $w_i \in \mathbf{R}^{2\times1}$. The detailed expressions are as follows and all variables in state-vector x_i are explained in Section 2.1.

$$x_i = \begin{bmatrix} x_{i1} & x_{i2} & x_{i3} & x_{i4} & x_{i5} & x_{i6} \end{bmatrix}^T = \begin{bmatrix} \Delta f_i & \Delta P_{gi} & \Delta P_{ri} & \Delta X_{ei} & \Delta P_{tiei} & \int ACE_i dt \end{bmatrix}^T$$

$$w_i = \begin{bmatrix} \Delta P_{ci} & 2\pi \sum_{i=1, i\neq j}^{n} T_{ij} \end{bmatrix}^T$$

The state space model of power system in *i*th control area can be established as follows:

$$\begin{cases} \dot{x}_i = A_i x_i + B_i u_i + F_i w_i \\ y_i = C_i x_i \end{cases} \tag{6}$$

where $A_i \in \mathbf{R}^{6\times6}$, $B_i \in \mathbf{R}^{6\times1}$, $F_i \in \mathbf{R}^{6\times2}$ and $C_i \in \mathbf{R}^{1\times6}$ are parameter matrices of system. Their expressions are as below:

$$B_i = \begin{bmatrix} -\frac{K_{pi}}{T_{pi}} & 0 & 0 & 0 & 0 & 0 \end{bmatrix}^T$$

$$C_i = \begin{bmatrix} -\frac{\beta_i}{R_i} & 0 & 0 & 0 & 0 & 0 \end{bmatrix}^T$$

$$F_i = \begin{bmatrix} -\frac{K_{pi}}{T_{pi}} & 0 & 0 & 0 & 0 & 0 \\ 0 & 0 & 0 & 0 & -2\pi & 0 \end{bmatrix}^T$$

$$A_i = \begin{bmatrix} -\frac{1}{T_{pi}} & \frac{K_{pi}}{T_{pi}} & 0 & 0 & -\frac{K_{pi}}{T_{pi}} & 0 \\ 0 & -\frac{1}{T_{ti}} & \frac{1}{T_{ti}} & 0 & 0 & 0 \\ -\frac{c}{T_{gi}}(\frac{1}{R_i} + K_{AFi}) & 0 & -\frac{1}{T_{ri}} & \frac{1}{T_{ri}} - \frac{c}{T_{gi}} & 0 & -\frac{c}{T_{gi}} \\ -\frac{1}{T_{gi}}(\frac{1}{R_i} + K_{AFi}) & 0 & 0 & -\frac{1}{T_{gi}} & 0 & -\frac{K_i}{T_{gi}} \\ 2\pi \sum\limits_{i=1, i\neq j}^{n} T_{ij} & 0 & 0 & 0 & 0 & 0 \\ \frac{\beta_i}{R_i} & 0 & 0 & 0 & 0 & 0 \end{bmatrix}$$

4. H_∞ State Feedback Controller Design for Power System with the HESS in the *i*th Control Area

Take the four-area interconnected power system as study object. The control block diagram designed for the *i*th control area is shown in Figure 6. P_{ci}^* is a given power instruction calculated by the H_∞ controller to the HESS. P_{ci} denotes the power flow provided to power system by the HESS. y_i is the output of power system in the *i*th control area which denotes the area control error (ACE). $x_{i1}, \ldots, x_{i6}$ ($i = 1, 2, 3, 4$) present six inner state quantities of the *i*th control area. The specific description and meaning of each state which have been given in Sections 2 and 3.

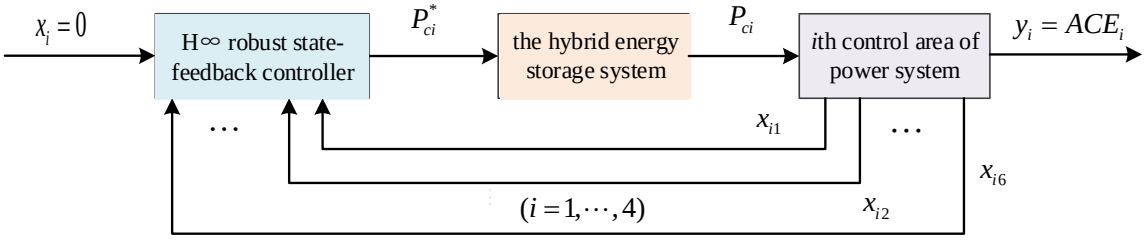

Figure 6. H_∞ robust state feedback control for the *i*th control area.

Combining the mathematical model (Equation (6)) of power system in *i*th control area with the control structure shown in Figure 6, the closed-loop system model of the *i*th control area can be expressed as follows:

$$\begin{cases} \dot{x}_i = A_i x + B_i u_i + F_i w_i \\ z_i = C_{1i} x + D_{12i} u_i \\ v_i = C_{2i} x_i \end{cases} \tag{7}$$

where w_i represents the disturbance signal consisting of ΔP_{ci} and $2\pi\sum_{i=1,i\neq j}^{n} T_{ij}$, which, respectively, represent the load disturbance and the interregional interaction. u_i is an input signal of system which is generated by the HESS, z_i is an evaluation signal and v_i is the observed signal of system. In this paper, we choose x_i as the observed quantity. C_{2i} is an identity matrix. A_i, B_i and F_i are coefficient matrices of the controlled object which are detailed described in Section 3. C_{1i} and D_{12i} are both weighted coefficient matrices. It should be noticed that, if the selection of C_{1i} or D_{12i} is not appropriate, there will be a bad influence on the control performance of the system. q_{ij} ($i, j = 1, \ldots, 6$) and ρ_i are weighting coefficients greater than zero. The definition of evaluation signal z_i is as follows:

$$z_i = \begin{bmatrix} q_{i1} & 0 & 0 & 0 & 0 & 0 \\ 0 & q_{i2} & 0 & 0 & 0 & 0 \\ 0 & 0 & q_{i3} & 0 & 0 & 0 \\ 0 & 0 & 0 & q_{i4} & 0 & 0 \\ 0 & 0 & 0 & 0 & q_{i5} & 0 \\ 0 & 0 & 0 & 0 & 0 & q_{i6} \\ 0 & 0 & 0 & 0 & 0 & 0 \end{bmatrix} x_i + \begin{bmatrix} 0 \\ 0 \\ 0 \\ 0 \\ 0 \\ 0 \\ \rho_i \end{bmatrix} u_i \tag{8}$$

The controller coefficient matrix K_i is designed satisfying the stability condition of (A_i, B_i, C_{2i}). The matrix D_{12i} in Equation (7) is required to be column full rank to make sure that the controller K_i is a real rational function matrix. The state feedback controller of power system in ith control area is designed as follows:

$$u_i = K_i x_i \tag{9}$$

Substituting Equation (9) into Equation (7), the corresponding expression can be obtained as follows:

$$\begin{cases} \dot{x}_i = (A_i + B_i K_i) x_i + F_i w_i \\ z_i = (C_{1i} + D_{12i} K_i) x_i \\ v_i = x_i \end{cases} \tag{10}$$

Aiming at the problem about robust stability and disturbance suppression performance of control system, the key of state feedback controller design by using H_∞ control theory lies in: solving appropriate state feedback controller promising the closed-loop system is stable and the H_∞ norm of the closed-loop transfer function matrix is minimum or less than a given value. Let T_{zw} be the transfer function from input w to output z. The goal of H_∞ design is guaranteeing the H_∞ norm of T_{zw} to be less than γ and it can be expressed as follows:

$$\|T_{zw}\| = \|(C_{1i} + D_{12i} K_i)[sI - (A_i + B_{2i} K_i)^{-1} B_{1i}]\| \tag{11}$$

The following three kinds of H_∞ controller design problems can be differentiated according to the selection of γ. If the state feedback controller *K(s)* can guarantee the closed-loop transfer function of the control system to be internally stable and the value of $\|T_{zw}\|_\infty$ is minimum. That is, $\|T_{zw}\|_\infty = \gamma_0$ and it is called H_∞ controller optimal design. If K_i satisfies the equation $\|T_{zw}\|_\infty = \gamma > \gamma_0$ based on satisfying the sufficient stability condition of (A_i, B_i, C_{2i}), then this kind of problem is H_∞ controller suboptimal design problem. If $\|T_{zw}\|_\infty = \gamma \leq 1$ exists, then the corresponding H_∞ controller standard design problem [31–33].

Then, the following linear matrix inequality is established considering Equation (11) and standard design problem of H_∞ controller design:

$$\begin{bmatrix} A_i X_i + B_{2i} W_i + (A_i X_i + B_{2i} W_i)^T & B_{1i} & (C_{1i} X_i + D_{12i} W_i)^T \\ B_{1i}^T & -I & 0 \\ C_{1i} X_i + D_{12i} W_i & 0 & -{\gamma_i}^2 I \end{bmatrix} < 0 \tag{12}$$

If there exists a set of feasible solutions X_i^* and W_i^* can ensure the above inequality holds true, then $u_i = W_i^* (X_i^*)^{-1} x_i$ is an H_∞ state feedback controller of the system and the controller coefficient matrix is $K_i = W_i^* (X_i^*)^{-1}$. The control coefficient matrix K_i can be obtained by using the MATLAB LMI toolbox, feasp() or mincx() function to solve the linear matrix inequality in Equation (12).

5. Simulation and Result Analysis

Taking the four-area interconnected power system as research object in this paper and each control area can be distinguished by setting different values to various parameter variables. In the case of Control Area 1, the parameter settings are shown in Table 1.

Table 1. Parameters in Control Area 1 of the interconnected power system.

T_{gi} (s)	T_{ri} (s)	T_{ti} (s)	R_i (Hz/p.u.Mw)	$T_{1j(j=1,2,3,4)}$ (s)
0.08	4.2	0.3	2.4	0.0707
K_{p1} (s)	T_{p1} (s)	c_1	β_1 (Hz/p.u.Mw)	K_{AF1}
120	20	0.35	0.425	1.1

The electrical simulations of interconnected power system for four control areas area carried out through Matlab 2012a/Simulink in following three different cases:

- Case 1: Traditional LFC, i.e., power system without the HESS.
- Case 2: Power system with the HESS and external PID controller [14,34].
- Case 3: Power system with the HESS and external H_∞ robust state feedback controller.

Set the simulation time to 100 s. To test the robust stability and the suppression ability of the control system under load disturbance, load interference is added to the power system in Control Area 1, as shown in Figure 7, which consists of step signal, ramp signal and sinusoidal signal [35]. It is worth pointing out that, when Area 1 is disturbed by load interference, the load frequency of power systems in the other three control areas will be affected through the tie-lines between each area.

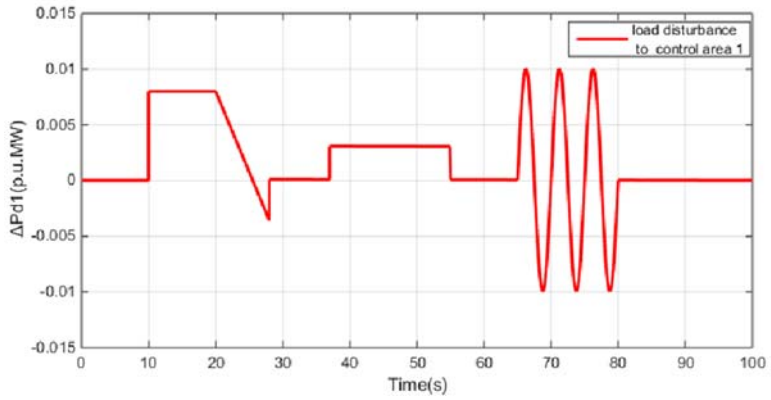

Figure 7. The external load disturbance added to Control Area 1.

Take the Area 1 as an example. In the process of H_∞ robust state feedback controller design, the weighting coefficients and performance indices are given as Table 2. Combining Section 4, the state feedback control coefficient matrix of Area 1 can be obtained by Matlab as K_1 = [−10.8625, 25.5883 5.2364, −8.8031, −7.6875, −9.2341] and coefficient matrices for other three control areas can be easily obtained by using the method above.

Table 2. Parameters of controller design for Control Area 1.

$(i=1)$	q_{i1}	q_{i2}	q_{i3}	q_{i4}	q_{i5}	q_{i6}	ρ_1	γ_1^2
Area 1	0.0125	0.01	0.001	0.005	0.001	0.013	0.09	0.86

For Case 3, Figure 8 shows the control signal u_1, u_2, u_3, u_4 for each control area from the H_∞ state feedback controller designed in this paper. These control signals denote the power instruction transmitted to the HESS from H_∞ controller. More attention should be paid to the magnitude order of the axis because they are different in each figure. It can be noticed that the orders of magnitude in Figure 8b–d are really small, respectively, 10^{-5}, 10^{-5} and 10^{-6}.

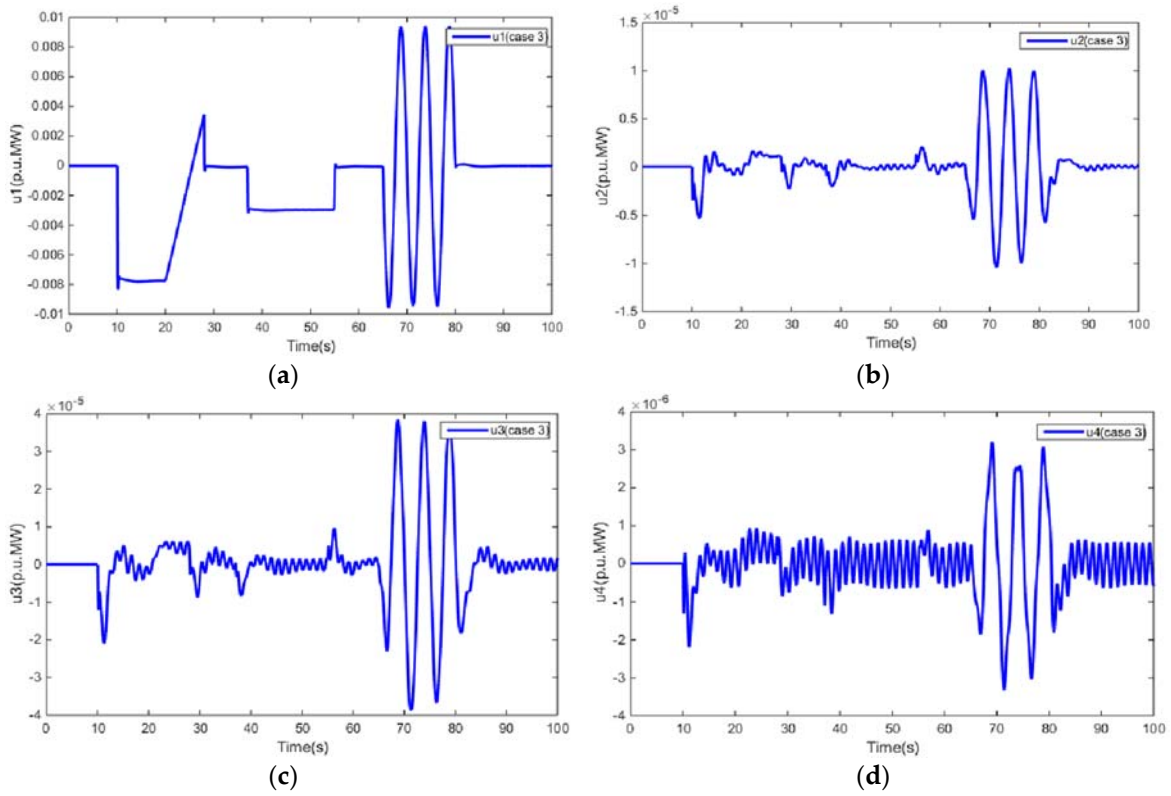

Figure 8. Control signals from controller of four areas in Case 3: (**a**) control signal u_1; (**b**) control signal u_2; (**c**) control signal u_3; and (**d**) control signal u_4.

Figure 9 shows the load frequency deviation $\Delta f_i (i = 1, 2, 3, 4)$ of each power system under load disturbance in Case 3. When the load disturbance of Figure 8 arises in Control Area 1, load frequencies of each power system will be subjected to varying degrees of influence. Under the condition of LFC with the HESS and external H_∞ robust state feedback controller, in Figure 8 we can see that the load frequency $f_i (i = 1, 2, 3, 4)$ restores stability rapidly in seconds and $\Delta f_i (i = 1, 2, 3, 4)$ was guaranteed to be within ± 0.0006 Hz since the maximum interference is almost 10 Kw. The result comparison of PID controller and H_∞ state-feedback controller is shown in Figure 10 under the condition of LFC with the HESS.

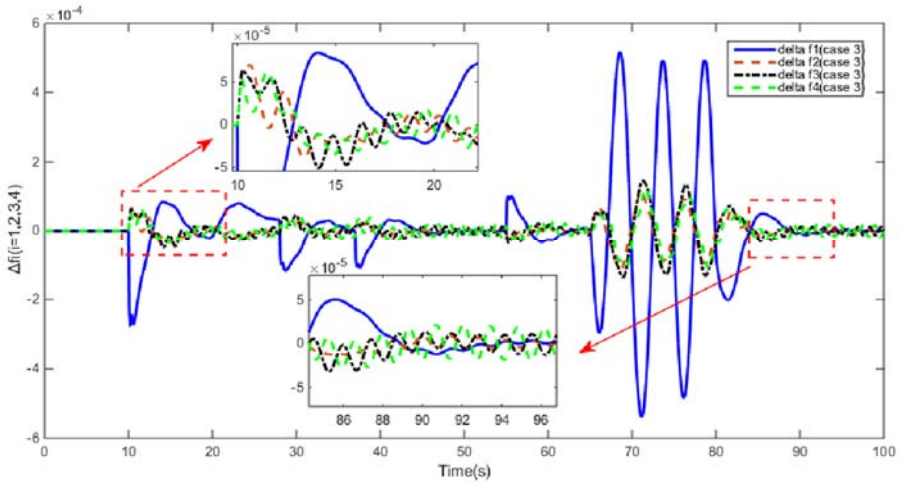

Figure 9. $\Delta f_i (i = 1, 2, 3, 4)$ of each power system under load disturbance in Case 3.

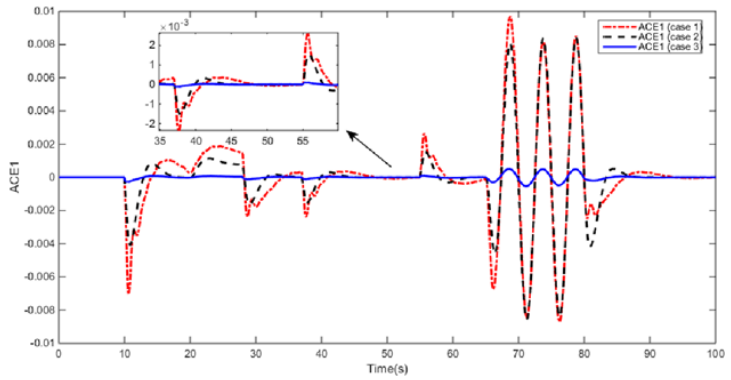

(**a**)

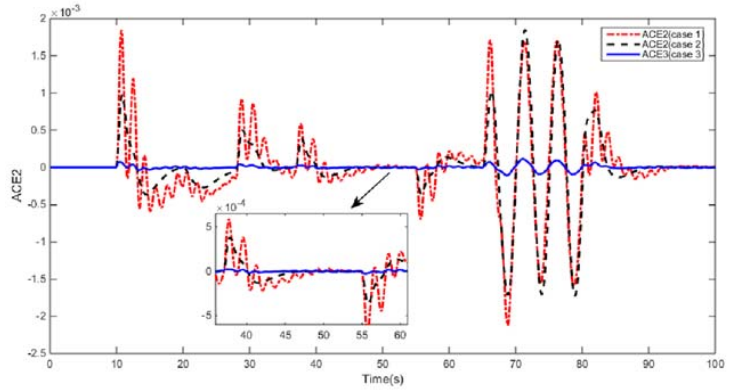

(**b**)

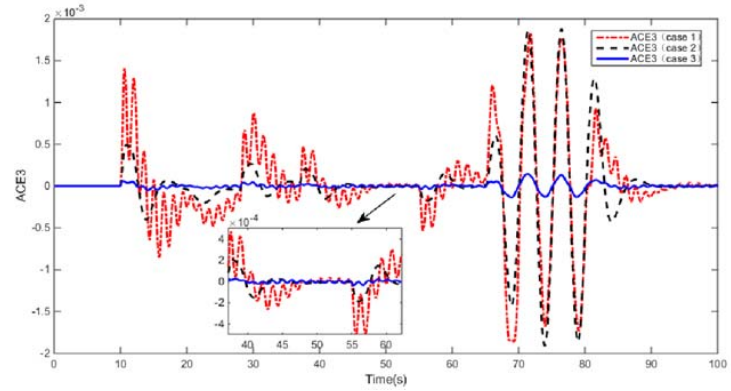

(**c**)

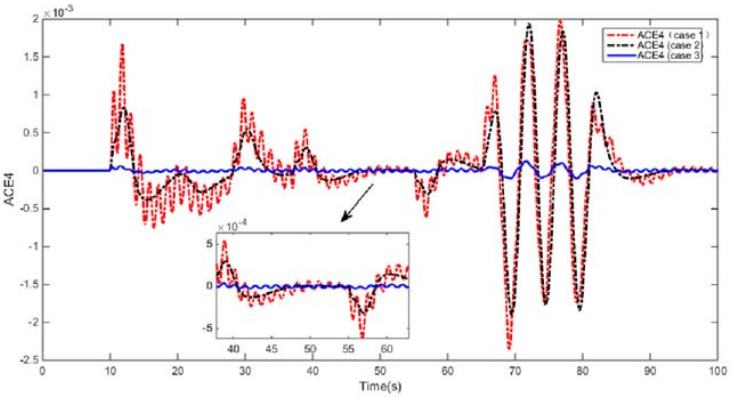

(**d**)

Figure 10. $ACE_i (i = 1, 2, 3, 4)$ of each control area under load disturbance in three different cases: (**a**) ACE_1 of Control Area 1; (**b**) ACE_2 of Control Area 2; (**c**) ACE_3 of Control Area 3; and (**d**) ACE_4 of Control Area 4.

Figure 10 shows the control effect comparison of four areas in three different situations. The control effect is evaluated according to whether the value of the reference performance index $ACE_i(i = 1, 2, 3, 4)$ is close to zero. The expression of $ACE_i(i = 1, 2, 3, 4)$ is composed of terms ΔP_{tiei} and Δf_i, $ACE_i = \Delta P_{tiei} + \varphi_i \Delta f_i$. The closer ACE_i is to zero, the better is the control effect. Figure 10a–d, respectively, shows the simulation results of the Control Areas 1–4 in three different cases.

Comparing and analyzing the output waveform of the system, when the load disturbance occurs in Case 1, the ACE_i values of each region oscillate greatly and it takes more time to recover the stability near the zero value. Comparing PID control and H_∞ robust state feedback control, it can be clearly seen in Figure 10 that H_∞ robust state feedback controller can effectively enhance the robustness and stability of the system in the condition of disturbance, keep the system output ACE_i fluctuating within the range of ± 0.0006 Hz near zero and restore the system frequency stability within 10 s.

The design goal of this paper is to return the stability of the load frequency of the power system as quickly as possible in the event of external load disturbances, namely, make the value of area control error (ACE_i) stable at zero or within a minimum range near zero. Therefore, through the analysis of simulation results, it can be shown that the stability of power system and the control performance of the LFC can be improved effectively by introducing the HESS.

6. Conclusions

This paper studies the problem of improving the frequency stability of multi-area interconnected power system and proposes that the HESS should be introduced to restrain the frequency fluctuation of the interconnected power network. The mathematical model of a single control system is established and H_∞ robust state feedback controller based on LMI is designed to further enhance the robustness and stability of the system for the LFC. Finally, the feasibility and effectiveness of the proposed scheme are proven by the simulation and results analysis. Moreover, the coupling problem in large power system is not considered and the study of coupling quantity in large area power system will be the next research direction.

Author Contributions: All authors contributed to designing and performing measurements, data analysis, scientific discussions, and writing the article.

Funding: This work was partially supported by the National Natural Science Foundation of China (61503156), National Key Research and Development Program (2016YFD0400301), Open Research Fund of Jiangsu Collaborative Innovation Center for Smart Distribution Network, Nanjing Institute of Technology (XTCX201806), National first-class discipline program of Food Science and Technology (JUFSTR20180205), and State Grid Zhejiang Province Technology Project (SGTYHT/17-JS-201)

Conflicts of Interest: The authors declare no conflict of interest.

References

1. Mi, Y.; Yang, Y.; Zhang, H. Sliding mode based load frequency control for multi-area interconnected power system containing renewable energy. In Proceedings of the 2014 IEEE Conference and Expo Transportation Electrification Asia-Pacific (ITEC Asia-Pacific), Beijing, China, 31 August–3 September 2014; pp. 1–6.
2. Fang, Z.; Zhao, H.G.; Liu, Z.H. The influence of large power grid interconnected on power system dynamic stability. *Proc. CSEE* **2007**, *27*, 1–7.
3. Gurrala, G.; Sen, I. Power system stabilizers design for interconnected power systems. *IEEE Trans. Power Syst.* **2010**, *25*, 1042–1051. [CrossRef]
4. Saikia, L.C.; Nanda, J.; Mishra, S. Performance comparison of several classical controllers in AGC for multi-area interconnected thermal system. *Int. J. Electr. Power Energy Syst.* **2011**, *33*, 394–401. [CrossRef]
5. Zuo, J.; Xie, P.; Li, Y. Intelligent optimization algorithm based load frequency controller design and its control performance assessment in interconnected power grids. *Trans. China Electrotech. Soc.* **2018**, *33*, 478–489.
6. Xu, D.Z.; Liu, J.; Yan, X.G. A novel adaptive neural network constrained control for multi-area interconnected power system with hybrid energy storage. *IEEE Trans. Ind. Electron.* **2018**, *65*, 6625–6634. [CrossRef]
7. Moorthi, V.R.; Aggarwal, R.P. Suboptimal and near-optimal control of a load-frequency-control system. *Proc. Inst. Electr. Eng.* **1972**, *119*, 1653–1660. [CrossRef]

8. Bengiamin, N.N.; Chan, W.C. 3-level load-frequency control of power systems interconnected by asynchronous tie lines. *Electr. Eng. Proc. Inst.* **1979**, *126*, 1198–1200. [CrossRef]
9. Bengiamin, N.N.; Chan, W.C. Multilevel load-frequency control of interconnected power systems. *Electr. Eng. Proc. Inst.* **1978**, *125*, 521–526. [CrossRef]
10. Talaq, J.; Al-Basri, F. Adaptive fuzzy gain scheduling for load frequency control. *IEEE Trans. Power Syst.* **1999**, *14*, 145–150. [CrossRef]
11. Farahani, M.; Ganjefar, S.; Alizadeh, M. PID controller adjustment using chaotic optimisation algorithm for multi-area load frequency control. *IET Control Theory Appl.* **2012**, *6*, 1984–1992. [CrossRef]
12. Khooban, M.H.; Niknam, T. A new intelligent online fuzzy tuning approach for multi-area load frequency control: Self-adaptive modified bat algorithm. *Int. J. Electr. Power Energy Syst.* **2015**, *71*, 254–261. [CrossRef]
13. Boroujeni, S.M.S.; Boroujeni, B.K.; Abdollahi, M. Multi-area load frequency control using PI controller tuned by particle swarm optimization. *Res. J. Appl. Sci. Eng. Technol.* **2011**, *3*, 1396–1401.
14. Zaki Diab, A.A.; EL-Satter, M.A. Adaptive model predictive based load frequency control in an interconnected power system. In Proceedings of the IEEE Conference of Russian Young Researchers in Electrical and Electronic Engineering (EIConRus), Moscow, Russia, 29 January–1 February 2018; pp. 604–610.
15. Menniti, D.; Pinnarelli, A.; Sorrentino, N. Coordinated control of phase shifters in multi-area power system to improve load-frequency dynamic performance. In Proceedings of the 16th IEEE Mediterranean Electrotechnical Conference, Yasmine Hammamet, Tunisia, 25–28 March 2012; pp. 241–244.
16. Song, X.; Deng, J.; Xu, D. Generic model control for hybrid energy storage system in electric vehicles. In Proceedings of the IECON 2017—43rd Annual Conference of the IEEE Industrial Electronics Society, Beijing, China, 29 October–1 November 2017; pp. 7151–7156.
17. Ma, M.; Liu, X.; Zhang, C. LFC for multi-area interconnected power system concerning wind turbines based on DMPC. *IET Gener. Transm. Distrib.* **2017**, *11*, 2689–2696. [CrossRef]
18. Singhparmar, K.P. LFC system of multi-area interconnected power systems using TVAC-PSO based controller. *Int. J. Comput. Appl.* **2014**, *88*, 13–19.
19. Pourmousavi, S.A.; Behrangrad, M.; Nehrir, M.H. LFC model for multi-area power systems considering dynamic demand response. In Proceedings of the IEEE/PES Transmission and Distribution Conference and Exposition, Dallas, TX, USA, 3–5 May 2016; pp. 1–5.
20. Ma, M.; Zhang, C.; Liu, X. Distributed model predictive load frequency control of the multi-area power system after deregulation. *IEEE Trans. Ind. Electron.* **2017**, *64*, 5129–5139. [CrossRef]
21. Shukla, R.R.; Patel, N.K. Effect of capacitive energy storage unit on frequency of interconnected multi-area power systems. In Proceedings of the 2018 Conference on Signal Processing and Communication Engineering Systems (SPACES), Vijayawada, India, 4–5 January 2018.
22. Mufti, M.U.D.; Lone, S.A.; Iqbal, S.J. Super-capacitor based energy storage system for improved load frequency control. *Electr. Power Syst. Res.* **2009**, *79*, 226–233. [CrossRef]
23. Farahani, M.; Ganjefar, S. Solving LFC problem in an interconnected power system using superconducting magnetic energy storage. *Phys. C Supercond. Its Appl.* **2013**, *487*, 60–66. [CrossRef]
24. Holland, C.E.; Weidner, J.W.; Dougal, R.A.; White, R.E. Experimental characterization of hybrid power systems under pulse current loads. *J. Power Sources* **2002**, *109*, 32–37. [CrossRef]
25. Khaligh, A.; Li, Z. Battery, ultracapacitor, fuel Cell, and hybrid energy storage systems for electric, hybrid electric, fuel cell, and plug-in hybrid electric vehicles: State of the art. *IEEE Trans. Veh. Technol.* **2010**, *59*, 2806–2814. [CrossRef]
26. Zhang, G.; Tang, X.; Zhiping, Q.I. Application of hybrid energy storage system of super-capacitors and batteries in a microgrid. *Autom. Electr. Power Syst.* **2010**, *299*, R1013–R1039.
27. Jiang, Q.; Hong, H. Wavelet-Based capacity configuration and coordinated control of hybrid energy storage system for smoothing out wind power fluctuations. *IEEE Trans. Power Syst.* **2013**, *28*, 1363–1372. [CrossRef]
28. Duong, M.Q.; Nguyen, V.T.; Sava, G.N.; Scripcariu, M.; Mussetta, M. Design and simulation of PI-type control for the buck boost converter. In Proceedings of the 2017 International Conference on ENERGY and ENVIRONMENT (CIEM), Bucharest, Romania, 19–20 October 2017; pp. 79–82.
29. Lukic, S.M.; Wirasingha, S.G.; Rodriguez, F. Power management of an ultra-capacitor/battery hybrid energy storage system in an HEV. In Proceedings of the 2006 IEEE Vehicle Power and Propulsion Conference, Windsor, UK, 6–8 September 2006; pp. 1–6.

30. Choi, M.E.; Kim, S.W.; Seo, S.W. Energy management optimization in a battery/supercapacitor hybrid energy storage system. *IEEE Trans. Smart Grid* **2012**, *3*, 463–472. [CrossRef]
31. Lei, H. H-infinity robust control of the suspension system for a bearingless motor of permanent magnet type. *Control Theory Appl.* **2008**, *25*, 711–716.
32. Wang, Z.Y.; Zhen, Z.; Zhou, K.M. Dynamic hysteresis modeling and H-infinity robust control of piezoelectric actuators. *Control Theory Appl.* **2014**. [CrossRef]
33. Yang, M.; Li, Y.; Du, H. Hierarchical multi-objective H-infinity robust control design for wireless power transfer system using genetic algorithm. *IEEE Trans. Control Syst. Technol.* **2018**, 1–9. [CrossRef]
34. Padhan, D.G.; Majhi, S. A new control scheme for PID load frequency controller of single-area and multi-area power systems. *ISA Trans.* **2013**, *52*, 242–251. [CrossRef] [PubMed]
35. Dullerud, G.E.; Paganini, F. *A Course in Robust Control Theory*; Springer: Berlin, Germany, 2000; Volume 36, p. B33.